

VTT Technical Research Centre of Finland

Impact of 15-day energy forecasts on the hydro-thermal scheduling of a future Nordic power system

Rasku, Topi; Miettinen, Jari; Rinne, Erkka; Kiviluoma, Juha

Published in:
Energy

DOI:
[10.1016/j.energy.2019.116668](https://doi.org/10.1016/j.energy.2019.116668)

Published: 01/02/2020

Document Version
Early version, also known as pre-print

[Link to publication](#)

Please cite the original version:

Rasku, T., Miettinen, J., Rinne, E., & Kiviluoma, J. (2020). Impact of 15-day energy forecasts on the hydro-thermal scheduling of a future Nordic power system. *Energy*, 192, [116668].
<https://doi.org/10.1016/j.energy.2019.116668>



VTT
<http://www.vtt.fi>
P.O. box 1000FI-02044 VTT
Finland

By using VTT's Research Information Portal you are bound by the following Terms & Conditions.

I have read and I understand the following statement:

This document is protected by copyright and other intellectual property rights, and duplication or sale of all or part of any of this document is not permitted, except duplication for research use or educational purposes in electronic or print form. You must obtain permission for any other use. Electronic or print copies may not be offered for sale.

Impact of 15-day energy forecasts on the hydro-thermal scheduling of a future Nordic power system

Topi Rasku^{a,*}, Jari Miettinen^b, Erkkä Rinne^a, Juha Kiviluoma^a

^a*VTT Technical Research Centre of Finland Ltd., P.O. Box 1000, FI-02044 VTT, Espoo, Finland*

^b*Fortum Corporation, P.O. Box 100, FI-00048 FORTUM, Espoo, Finland*

Abstract

One of the most promising ways of de-carbonising the energy sector is through increasing the amounts of variable renewable energy (VRE) generation in power systems. While the inherent uncertainty of VRE is a challenge, it can be mitigated through improved forecasting and energy system modelling. Typically, stochastic energy system studies have focused on the day-ahead horizon of 36 hours ahead of time, while studies about hydro-thermal scheduling and expansion planning often neglect VRE uncertainty entirely. In this work, the potential benefits of extending the horizon of VRE forecasts on the operation of hydro-dominated power systems was examined using a future Nordic system case study. 15-day ensemble weather forecasts were processed into realistic VRE and demand forecasts up to 348 hours ahead of time, and their impact on power system operations was simulated using stochastic unit commitment and economic dispatch optimisation. While decreases in total yearly operational costs, hydropower spillage and wind power curtailment were observed until forecast horizons up to around 132–156 hours ahead of time, the relative reductions remained rather insignificant at around 0.20–0.35 % for the costs, and 0.10 pp for the spillage and curtailment.

Keywords: Unit commitment, Economic dispatch, Hydro-thermal scheduling, Stochastic programming, Energy forecasting

*Corresponding author

Email address: `topi.rasku@vtt.fi` (Topi Rasku)

1 Nomenclature

- 2 ED Economic dispatch
- 3 FDIR Total sky direct solar radiation at surface
- 4 MAE Mean absolute error
- 5 MEUR Million euros
- 6 O&M Operations and maintenance
- 7 pp Percentage point
- 8 PV Photovoltaic
- 9 SSRD Surface solar radiation downwards
- 10 TYNDP Ten Year Network Development Plan
- 11 UC Unit commitment
- 12 VRE Variable renewable energy

13 1. Introduction

14 Mitigating climate change is a major driver increasing the amount of vari-
15 able renewable energy (VRE) in power systems around the globe. Weather
16 dependent VRE resources increase the uncertainty in the power system, af-
17 fecting both the system operators trying to ensure the balance of generation
18 and load, as well as the electricity market participants trying to decide their
19 optimal bids. Thus, dealing with VRE uncertainty via improved weather
20 forecasting and new energy system modelling approaches has been receiving
21 increasing interest.

22 Better generation forecasts for VRE have long been valuable in power
23 markets. As a result, there is a considerable amount of literature about the
24 various forecasting methods [1, 2], as well as their role in renewable energy
25 integration [3, 4, 5] and microgrid management [6]. In recent years, the
26 focus of energy forecasting has shifted from deterministic approaches towards
27 probabilistic ones [7], in order to better represent the underlying uncertainty
28 in power systems with significant amounts of VRE generation.

29 The increasing role of VRE resources has also emphasised stochastic mod-
 30 elling of the power system, over more traditional deterministic modelling
 31 approaches [8, 9, 10]. Existing literature has studied the impact of differ-
 32 ent wind power uncertainty representations on a two-stage stochastic unit
 33 commitment (UC) and economic dispatch (ED) problem [11], the energy
 34 market value of improving the accuracy of short-term wind power forecasts
 35 [12], as well as how the economic and reliability impacts of such forecast im-
 36 provements depend on the generation mix and energy storage capacity of the
 37 simulated power system [13]. Recently, Bakirtzis et al. presented a stochas-
 38 tic unified UC&ED model for short-term power system scheduling with a
 39 variable time resolution, and used it to study the benefits of stochastic over
 40 deterministic scheduling [14], as well as the optimal scheduling of energy stor-
 41 ages under short-term uncertainty [15]. Overall, most of the literature agrees
 42 that stochastic UC&ED results in lower costs and more robust solutions com-
 43 pared to deterministic approaches, but cautions that the magnitude of the
 44 benefits are dependent on the generation mix and energy storage capacity.

45 All of the above-mentioned studies have focused on the short-term schedul-
 46 ing within common day-ahead market horizons of up to around 36–48 hours
 47 ahead of time, which is reasonable for systems without longer-term energy
 48 storage. However, in power systems with such storage, e.g. in the form of
 49 large hydropower reservoirs or district heating system scale hot water storage,
 50 considering the uncertainty in VRE generation beyond the day-ahead horizon
 51 might have an impact on the optimal scheduling of the system. Surprisingly,
 52 literature about the impact of using longer wind and solar power forecasts
 53 seems to be much harder to find. While optimisation horizons ranging from
 54 weeks to months and even years are common in hydro-thermal scheduling
 55 and expansion planning [16], the short-term uncertainty associated in VRE
 56 production is either not represented adequately for dispatch, or is neglected
 57 entirely.

58 Previous approaches to long-term hydro-thermal scheduling have consid-
 59 ered the uncertainty of wind power on the weekly [17, 18] or monthly [19]
 60 time scales, but resort to deterministic dispatch within these time scales in
 61 order to reduce the computational burden. Some studies have also focused on
 62 short-term hydro-thermal scheduling using a robust approach under severe
 63 load uncertainty [20], as well as with improved technical modelling of pumped
 64 hydro units [21]. However, these studies again focus on optimal scheduling
 65 on the day-ahead horizon of only 24 hours. The impact of varying forecast
 66 lengths on the operation of power systems has been recently studied by Erich-

set et al. [22], focusing on the CO₂ emissions of an electricity producer park with long-term energy storage. The tested horizons were chosen to represent possible weather forecast ranges 2–14 days ahead, as well as a hypothetical 30 day forecast and a full 365 day perfect horizon. However, the used UC model was deterministic with perfect foresight for all tested horizons, and the use of the long-term energy storage was determined by simple heuristics instead of it being included the UC optimisation.

This paper aims to study the impact of extended weather forecasts on the operational costs of hydro-dominated power systems by using a Nordic case study with actual ensemble weather forecast data in a rolling stochastic unified UC&ED optimisation model. We hypothesise that by utilising weather forecasts beyond the day-ahead horizon, the operational costs of the power system could be reduced further via improved co-scheduling of VRE and hydropower resources. While only hydropower is featured in the chosen case study, similar benefits could be possible with any form of sufficiently long-term energy storage solutions, and potentially even in power systems with significant amounts of slow response thermal power plants. A previous study by the authors [23] is improved upon by including forecasts for solar generation, as well as electricity and heat demands in addition to wind power forecasts. Furthermore, the impact of the modelled forecast horizon is studied until the full 15-day ahead horizon of the ensemble weather forecast data in a more accurate depiction of the Nordic power system.

Section 2 explains all the data and methods used for constructing the hypothetical future Nordic power system, processing the weather ensemble forecasts, as well as the used stochastic UC model. The results of power system simulations with a number of different forecast horizons and time resolutions are presented in Section 3, and the findings are discussed in Section 4. Finally, main conclusions are drawn and summarised in Section 5.

2. Materials and Methods

In order to study the impact of extended weather forecasts on hydro-thermal scheduling, a hypothetical future Nordic power system was constructed based on existing scenario data, as detailed in Section 2.1. Furthermore, large amounts of weather data were aggregated, converted into energy terms, and calibrated as explained in Section 2.2. Only after all the desired power system and weather data had been properly processed, the impact of the extended VRE forecasts on the operational costs of the power system

Table 1: Installed electricity generation capacities by country and energy source, as well as the yearly electricity and heat demands.

	Installed capacity [GW]								Demand [TWh/a]	
	Solar	Wind	Hydro	Biomass	Nuclear	Coal& Lignite	Gas	Oil	Electricity	Heat
DE	64.0	67.2	5.9	6.9	0.0	36.8	27.0	1.3	559.0	121.6
DK	0.8	6.5	0.0	2.9	0.0	1.5	1.0	0.2	35.7	30.0
EE	0.0	0.5	0.0	0.2	0.0	1.4	0.3	0.0	8.3	6.1
FI	0.0	2.9	3.5	3.3	3.4	1.8	3.2	0.6	83.9	45.8
LT	0.1	0.5	0.1	0.1	1.1	0.0	1.4	0.0	10.2	9.9
LV	0.0	0.3	1.6	0.1	0.0	0.0	1.1	0.0	8.1	6.7
NO	0.0	2.4	41.8	0.0	0.0	0.0	0.6	0.0	135.7	6.8
PL	0.1	10.3	1.0	2.1	0.0	20.7	5.4	0.2	168.3	91.3
SE	0.1	9.0	16.7	3.2	7.0	0.1	3.3	0.5	144.2	51.8

could be simulated. A generic energy network optimisation tool called Backbone [24] was used to set up a rolling stochastic unified UC&ED model for optimising the power system operations, briefly described in Section 2.3.

2.1. Nordic case study

The modelled Nordic power system included the countries around the Baltic sea, with the exceptions of excluding Russia and including Norway, as shown in Figure 1. The European Reference Scenario 2016 [25] results for the year 2030 were used for the country-level power and heat generation capacities, as well as their annual energy demands. The resulting country-wise generation capacities, as well as the yearly electricity and heat demands, are presented in Table 1. Similarly, the total transmission capacities between countries were based on the “NTC 2027 reference grid” in the Ten Year Network Development Plan (TYNDP) 2018 [26]. In order to get a finer depiction of the power system, the e-Highway 2050 project [27] “Large scale RES” scenario for the year 2030 was used as the base for the regional division seen in Figure 1, and the generation and transmission capacities within the countries were distributed accordingly. However, Germany and Poland were still represented by single country-wide regions to reduce the complexity of the model, as they were mostly included to provide a more realistic depiction of electricity trading between the Northern and Central European power systems.

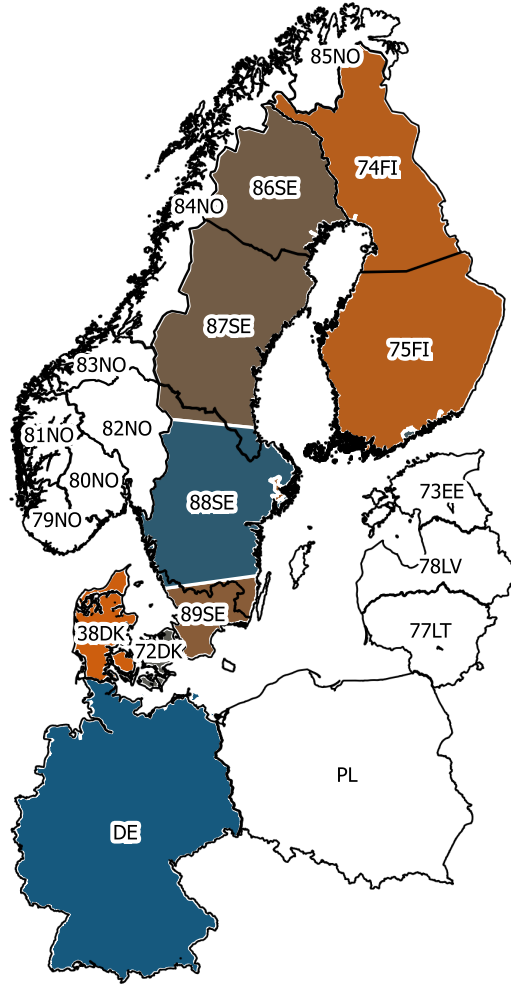


Figure 1: Illustration of the scope of the modelled Nordic power system, and its division into individual regions. The WILMAR project [28] heat areas used for generating the heat demand time series are shown in colour.

124 Fuel and carbon prices were obtained from the TYNDP 2018 [26] Market
125 Modelling Data “2030 EUCO” scenario, and the CO₂ content of the fuels
126 were based on IPCC guidelines [29]. However, as biomass and biofuel prices
127 weren’t available in the TYNDP 2018 data, estimated future prices from a
128 report by Pöyry Management Consulting Ltd [30] were used for biomass in-
129 stead. The cost of heating fuels were also increased by applying the minimum
130 excise duty rates as required by the European Union [31].

131 The technical parameters of the modelled power plants were based on
132 the TYNDP 2018 Market Modelling Data [26], and the required amounts of
133 frequency containment and restoration reserves in the Nordic countries were
134 based on the Nordic System Operation Agreement [32] with the assumption
135 that the new Olkiluoto 3 nuclear power plant becomes the dimensioning fault
136 in the Nordic power system. The reserve requirements in the remaining coun-
137 tries were estimated based on the Continental Europe Operation Handbook
138 [33] parts P1 and A1. Replacement reserves were not included, as they are
139 not used in the Nordic power system.

140 *2.1.1. Electricity and heat demand time series*

141 While the yearly demand for electricity and heat in Table 1 were based
142 on the European Reference Scenario 2016 [25] and e-Highway [27] results, the
143 hourly profiles were generated based on data from ENTSO-E transparency
144 platform [34] for electricity demand, and from the WILMAR project [28]
145 for heat demand. Instead of using the electricity and heat demand time
146 series from the aforementioned sources directly, demand models detailed in
147 Appendix A were used in order to generate demand forecasts based on
148 the weather forecast data discussed in Section 2.2. Unfortunately, the heat
149 demand data was only available for the areas shown in Figure 1, and the heat
150 demand for the remaining regions was estimated using models parameterised
151 with the existing data.

152 *2.1.2. Hydropower inflow time series*

153 Inflow data for hydropower reservoirs and run-of-river hydropower sta-
154 tions was collected from various sources. Weekly inflow time series used
155 for Norway and Sweden were originally simulated using EMPS [35]. The
156 dataset was provided by SINTEF Energi AS (“Hydropower inflow for Nor-
157 way and Sweden, 1958–2015”, received 24 October 2018). The EMPS areas
158 were mapped to their corresponding regions, and the weekly inflow energies
159 were divided into regulated inflow into reservoirs, and unregulated inflow into

Table 2: Variables used from ERA5 and ENS datasets. SSRD is the surface solar radiation downwards and FDIR is the total sky direct solar radiation at surface (srf). The used model levels are indicated using braces, and roughly correspond to altitudes of 107 m and 170 m.

variable	ERA5	ENS
wind speed [m/s]	100 m, {86, 87}	100 m, {130, 132}
temperature [K]	{srf, 86, 87}	{srf, 130, 132}
pressure [Pa]	{srf}	{srf}
SSRD _{acc} [J/m ²]	{srf}	{srf}
FDIR _{acc} [J/m ²]	{srf}	{srf}
a [Pa]	336.77 {86}	302.48 {130}
	162.04 {87}	122.10 {132}
b [–]	0.97 {86}	0.98 {130}
	0.98 {87}	0.98 {132}

run-of-river hydropower stations. The data was re-sampled to hourly resolution using linear interpolation, and the values were normalised to the annual totals from the European Reference Scenario 2016 [25]. Unfortunately, data for the year 2017, which was used as the weather data in Section 2.2, was not available for the entire modelled area and data from 2012 was used instead. Inflow data for Finland was derived from volumetric inflows from Finnish Environmental Administration [36], and inflows for the rest of the regions were based on data from the WILMAR project [28], again for the year 2012.

2.2. Weather data manipulation

The weather in the simulation was described using ERA5 [37] weather reanalysis data for the year 2017. ERA5 provides a great source of data for energy system modelling, including all spatial and temporal correlations which are paramount for modelling the impacts of VRE generation on the operation of energy systems. As for the weather forecast data, the ENS 15-day ensemble forecasts [38] were used, again for the year 2017. The data was obtained from the surface level and the model levels roughly corresponding to altitudes of 107 m and 170 m, as shown in Table 2 along with the other relevant parameters. Since the model levels are pressure based, the exact altitudes of the model levels vary depending on the surface temperature, and the aforementioned heights were estimated under fixed conditions.

180 *2.2.1. Wind power conversion*

181 In order to calculate the wind power production, the wind speeds must
 182 first be estimated for the assumed hub heights. The height h_l at different
 183 model levels l could be estimated using the equation [39]

$$h_l = \frac{T_{\text{srf}}}{L} \left[\left(\frac{p_l}{p_{\text{srf}}} \right)^{-\frac{LR}{g}} - 1 \right], \quad (1)$$

184 where T_{srf} is the surface temperature, L is the atmospheric lapse rate of
 185 temperature, p_l is the pressure at model level l , p_{srf} is the pressure at the
 186 surface, R is specific gas constant and g is the gravitational constant. All the
 187 variables in Equation (1) depend on both the coordinates as well as time. In
 188 the case of a ENS-data, the variables also depend on the analysis time of the
 189 forecast and the ensemble member. The pressure p_l could be calculated by
 190 applying model level dependent regression coefficients a and b in Table 2 to
 191 equation

$$p_l = a_l + b_l p_{\text{srf}}. \quad (2)$$

192 The wind speed at altitude h was estimated using wind profile power law

$$w_h = w_r \left(\frac{h}{h_r} \right)^\alpha, \quad (3)$$

193 where w_r and h_r are the reference wind speed and altitude, and α is the
 194 profile exponent defined by equation

$$\alpha = \frac{\log(w_{l[\text{low}]} / w_{l[\text{high}]})}{\log(h_{l[\text{low}]} / h_{l[\text{high}]})}, \quad (4)$$

195 where the low and high subscripts refer to the model level number presented
 196 in Table 2. Due to the fluctuating height of the ERA5 and ENS model
 197 levels, the reference wind speeds w_r were obtained from fixed reference height
 198 $h_r = 100$ m for calculating the wind speeds for the assumed average wind
 199 turbine hub height of 140 m.

200 After the wind speeds are know, the conversion into wind power produc-
 201 tion $P(w_h)$ is mainly dependent on two components: the wind resource at
 202 the the power plant site, and the technological parameters of the used wind
 203 turbines. These components can be combined into a power curve equation

$$P(w_h) = P_{\text{pc}}(Sr, c_p, \rho, w_h, w_{\text{cut-off}}, w_{\text{cut-off}, \Delta}), \quad (5)$$

where Sr is the specific rating, c_p is the coefficient of performance, ρ is the air density, w_h is the wind speed at hub height h , $w_{\text{cut-off}}$ is the cut-off wind speed and $w_{\text{cut-off},\Delta}$ is the associated hysteresis wind speed range for running down the power plant. Equation (5) used a Gaussian filter to smooth the wind speeds according to the methodology in [40] in order to account for the resolution of the weather data and unknown turbulence intensities, and is explained in detail in Appendix B.

2.2.2. Photovoltaic conversion

A method by Pfenninger et al. [41] was used for converting ERA5 and ENS weather data to production capacity factors for solar photovoltaic (PV) panels. Unlike [41], however, the downward component of the direct irradiation (FDIR) and the total diffuse irradiation were used as inputs, and the diffuse irradiation was simply calculated as the difference of surface solar radiation downwards (SSRD) and FDIR. Furthermore, it was assumed that the panels were crystalline silicon with 10 % total system losses, and the panels were rooftop installed with no tracking capability.

The tilt and azimuth angles were again based on [41], with the tilt angle of the panels β following the normal distribution

$$\beta \sim \mathcal{N}(-9.06 + 0.78\phi, (15^\circ)^2), \quad (6)$$

with the mean tilt angle depending on the current latitude ϕ , while the standard deviation was assumed to be 15° . Similarly, the azimuth angle γ followed

$$\gamma \sim \mathcal{N}(180^\circ, (40^\circ)^2), \quad (7)$$

where the mean azimuth angle of the panels was assumed to face south at 180° , and the standard deviation of the azimuth angles was assumed to be 40° .

2.2.3. Forecast calibration

As the realised and forecast data were obtained from different data sources, the ensemble forecasts had to be calibrated in order to minimise any bias error. In order to reduce the computational burden, the bias was minimised for the modelled regions only, instead of calibrating the forecasts in every coordinate point separately. First, the aggregated capacity weighted regional time series of wind speed and irradiation were calculated for both the ERA5 and the ENS data based on the regional capacities and the assumed

236 power plant locations presented in Figure 2. The locations of most of the wind
 237 power plants were based on the wind power plant database [42], including
 238 power plants currently under development. However, data from [43] was used
 239 for Germany and Denmark for both wind and PV installations. For the rest
 240 of the regions, geospatial data for the solar PV installations was not available.
 241 Instead, the locations were estimated by clusterising the population density,
 242 and using the centre points of the resulting clusters. The weight used for the
 243 regional aggregation was the population density of the cluster, multiplied
 244 with the cluster area. The population density clustering was also used for
 245 weighting the temperature data for the heat and electricity demand models
 246 explained in Appendix A.

247 In order to remove the bias error, the hourly median of the ensemble
 248 spread was calculated. Then, the error between the ERA5 data and the ENS
 249 data ensemble median ϵ_τ at horizon τ was represented using a generalised
 250 additive model

$$\mathbb{E}[\epsilon_\tau] = f_1(\tau) + f_2(H_\tau) + \beta_0, \quad (8)$$

251 where $f_{1,2}$ are penalised B-splines functions, which all have 20 basis functions,
 252 H_τ is the hour of the day at horizon τ , and β_0 is a constant. The pyGAM
 253 package [44] was used to solve Equation (8) for the suitable regression func-
 254 tions for correcting the forecast data. Finally, each ensemble member e was
 255 corrected using the obtained error

$$Y_{e,\tau}^{\text{corr}} = Y_{e,\tau}^{\text{raw}} - \epsilon_\tau, \quad (9)$$

256 where Y is the regionally aggregated weather quantity being corrected, namely
 257 wind speed, solar irradiation, or temperature. Figure 3 presents the bias and
 258 mean absolute error (MAE) of wind speed and SSRD in Germany before and
 259 after the bias correction.

260 Since including the entire set of 50 ensemble forecasts into a large scale
 261 power system model was computationally infeasible, the number of the fore-
 262 casts needed to be reduced. The 20 %, 50 % and 80 % quantiles of the en-
 263 semble spread were used to represent the range of uncertainty in the power
 264 system model in order to guarantee a certain spread in the forecasts at all
 265 times. Figure 4 presents an example of the final wind power capacity factor
 266 quantile forecasts in Southern Finland, and the spread of the quantiles can
 267 clearly be seen to increase as the forecast horizon increases.

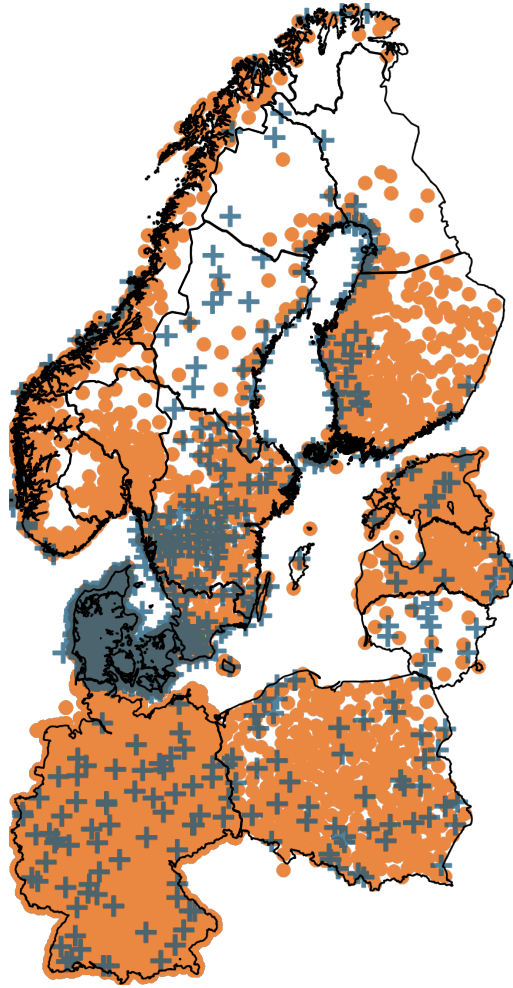


Figure 2: Illustration of the assumed wind and solar power plant locations. Wind power locations are denoted using blue crosses and solar power locations are denoted using orange disks. Geospatial data for solar in Germany and wind in Denmark was abundant, making individual sites indistinguishable in the figure.

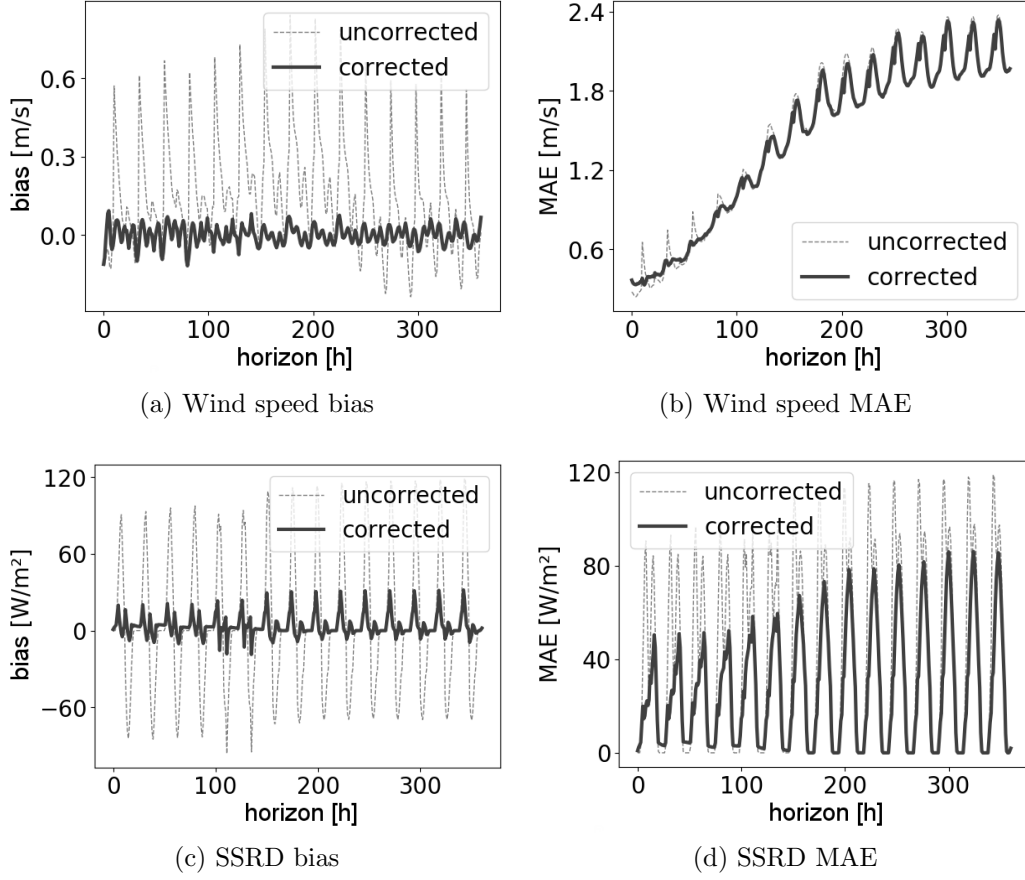


Figure 3: SSRD and wind speed bias and MAE on different forecast horizons for Germany before and after the bias correction.

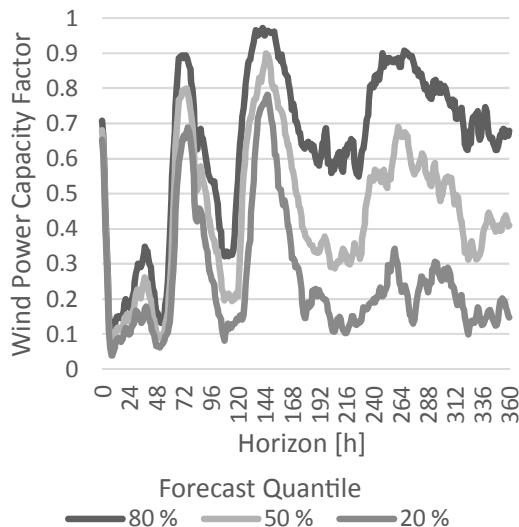


Figure 4: An example of the final wind power capacity factor quantile forecasts for the first two weeks of the simulation in Southern Finland.

2.3. Power system simulation

The rolling stochastic hydro-thermal scheduling of a future Nordic power system was performed using an open source mixed-integer linear programming-based generic energy network optimisation tool called Backbone [24]. The exact version of Backbone used in this work has been tagged as “VaGeResults” in the online repository [45].

The scheduling problem was formulated into a unified UC&ED model reminiscent of [14], but intended for longer modelling horizons required by reservoir hydropower and the extended weather forecasts. Figure 5 presents an illustration of the stochastic structure of a single solve in the rolling optimisation, after which the solution for the first six hours was recorded and the model was solved again starting six hours later in time. The first six hours of each solve represent the operational dispatch of the power system, where the power system has perfect information and dispatches itself accordingly. From the seventh hour up until the desired forecast horizon, the power system has to rely on the uncertain quantile forecast information to commit reserves for the next solve, as well as how to prepare to operate the system in general. The quantile forecasts were updated every 24 hours of model time, as new information became available. In order to reduce the computational burden, the time resolution of the model is progressively decreased

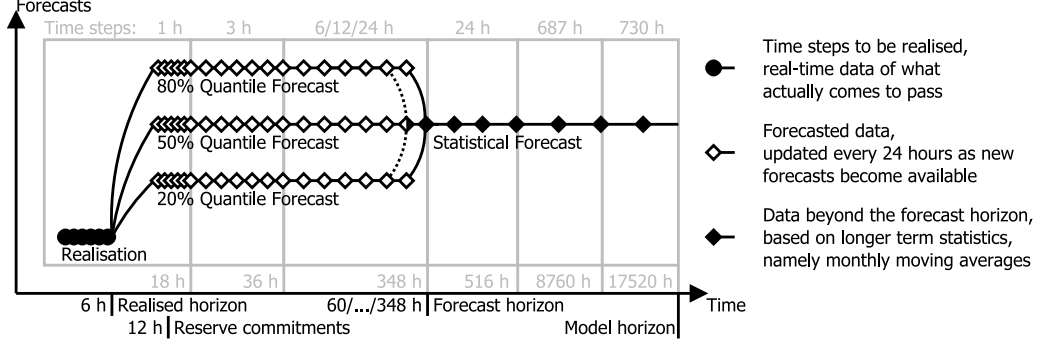


Figure 5: Illustration of the forecast-time structure of a single solve of the unified UC&ED optimisation. The dotted lines demonstrate the changes in the structure and data when the forecast horizon is varied between simulations.

beginning on the nineteenth hour, first to three hour time steps, and then even further as shown in Figure 5. The time resolution from the 36th hour until the 348th hour was varied between 6, 12, and 24 hours to determine whether the chosen time resolution has a significant impact on the results. From the forecast horizon until the end of the model horizon at 17,520 hours, the three quantile forecasts converge into a single deterministic forecast using statistical monthly averages.

The impact of extending the VRE forecasts was studied by varying the length of the period when the model used the quantile forecast data before transitioning into the long-term statistical data, as illustrated in Figure 5. The modelled forecast horizons included the 36 hours ahead horizon as a baseline, and each subsequent horizon every 24 hours until the longest modelled forecast horizon of 348 hours ahead. These horizons were chosen to take full advantage of the ENS 15-day ensemble weather forecast data discussed in Section 2.2.

The objective function used in the unified UC&ED problem

$$v^{\text{objective}} = \sum_{f,t} \left[p_{f,t}^{\text{probability}} \left(\sum_u \left[c_u^{\text{startup\&emission}} v_{u,f,t}^{\text{startup}} + (c_u^{\text{O\&M}} v_{u,f,t}^{\text{generation}} + \sum_{F \in \mathbf{F}_u} [c_{u,F}^{\text{fuel\&emission}} v_{u,F,f,t}^{\text{fuelUse}}]) \Delta_t \right) \right] \right] \quad (10)$$

aimed to minimise the *objective* variable representing the total expected operational costs of the power system over all forecasts f and time steps t .

Each forecast-time step was assigned a *probability* parameter, assumed to be 0.6 for the 50 % quantile forecast, 0.2 for both the 80 % and 20 % quantile forecasts, and 1.0 for both the realisation and the long-term statistical forecast. The *startup&emission* cost parameter included all the operational and maintenance, fuel, and emission related costs associated with the unit *startup* variable, while the operations and maintenance (*O&M*) and *fuel&emission* cost parameters were handled separately along with the unit energy *generation* and *fuelUse* variables respectively. As the *generation* and *fuelUse* variables represent average power during time step t , they were multiplied with the length of the time step Δ_t to obtain the total costs over the time step. The presented objective function in Equation (10) has been simplified from its full formulation in [24] for clarity by omitting grid and node dimensions, as well as all unused terms. In the model, nodes represent points for calculating energy balance, while grids are used to group nodes with the same energy carrier together.

The hydropower reservoirs were modelled as simple energy equivalent aggregate reservoirs, one for each of the modelled power system region with reservoir hydropower. The dynamics of the reservoirs were governed by the generic energy balance equation

$$\begin{aligned}
v_{n,f,t}^{state} - v_{n,f,t-1}^{state} = & \left(\sum_{n' \in \mathbf{N}_n} [(1 - p_{n',n}^{\text{transferLoss}}) v_{n',n,f,t}^{\text{transfer}} - v_{n,n',f,t}^{\text{transfer}}] \right. \\
& \left. + \sum_{u \in \mathbf{U}_n} [\pm v_{n,u,f,t}^{\text{generation}}] - v_{n,f,t}^{\text{spill}} \pm \tau_{n,f,t}^{\text{influx}} \right) \Delta_t \quad (11) \\
& \forall \{n, f, t\},
\end{aligned}$$

where the *state* variables were used for keeping track of the amount of energy stored in the reservoir nodes, and water inflow was represented using the *influx* time series. The reservoir nodes were not connected to any other nodes via *transfer* variables, but were able to spill excess energy using the *spill* variable. The *generation* variable and the *influx* time series are included in Equation (11) using a \pm for clarity, as they can be both positive and negative depending on the desired application. The set \mathbf{N}_n contains all nodes n' connected to node n via energy *transfer* variables, and the set \mathbf{U}_n contains all the units u that either output energy to node n , or draw energy from it as input using the *generation* variable. The *transferLoss* parameter was simply assumed to be 0.01 for all transmission lines, regardless of their capacity or length. The presented Equation (11) has been simplified from its full

337 formulation in [24] by omitting the grid dimension, as well as all unused
 338 terms. Run-of-river hydropower was aggregated similarly to the reservoir
 339 hydropower, except that no *state* variables were used in Equation (11) as
 340 run-of-river power plants were assumed to lack significant amounts of storage.

341 Equation (11) was also used for ensuring the balance of the power and
 342 heat systems by removing the *state* and *spill* variables, essentially reducing
 343 the equation to a power balance constrain instead. The *transfer* variables
 344 represented power transmission in the power grid, and the *influx* time series
 345 represented the power and heat demands. Neither power nor heat nodes were
 346 allowed to use the *spill* variable to get rid of excess energy in the system.

347 Further constraints were implemented to restraint power transmission ca-
 348 pacities, reserve balance and provision, as well as unit conversion efficiencies
 349 and online dynamics. These constraints are not presented here, however, as
 350 they are not crucial for understanding this study. Instead, interested read-
 351 ers are instead encouraged to take a look at the full model methodology
 352 presented in [24].

353 3. Results

354 The impact of extended weather forecasts on the operation of the mod-
 355 elled Nordic power system was studied by performing full year rolling stochas-
 356 tic unified UC&ED simulations using different forecast horizons. The time
 357 resolution between the 36th hour and the 348th hour of each solve was re-
 358 duced to improve computational performance, and the power system sim-
 359 ulations were carried out using time resolutions of 6 hours, 12 hours, and
 360 24 hours. The total computational time of the simulations was 27–77 hours
 361 when using the 6-hour time resolution depending on the modelled forecast
 362 horizon length, and 18–24 hours using a 24-hour time resolution on a Intel®
 363 Xeon® CPU E5-2620 @ 2.00 GHz using GAMS 24.0.2. The simulations with
 364 the 12-hour time resolution took around 17–30 hours depending on the mod-
 365 elled forecast horizon, but were run on Intel® Xeon® CPU W3690 @ 3.47
 366 GHz using GAMS 24.1.3 instead, so the computational times are not directly
 367 comparable.

368 Figure 6 presents the total yearly operational costs of the simulated power
 369 system as a function of the modelled forecast horizon, as well as the differ-
 370 ent cost components, with all the simulated forecast time resolutions. As
 371 hypothesised, the total operational costs of the power system could be seen
 372 to decrease as the modelled forecast horizon increases, but only until around

132–156 hours ahead. Interestingly, the total fuel and emission costs of the power system increased at forecast horizons above 132 hours, while the O&M and startup costs of the units maintained a slight decreasing trend. Overall, the total operational cost savings achieved by increasing the forecast horizon remain rather modest, only around 0.20–0.35 % (58–99 MEUR) per year. The total yearly CO₂ emissions behaved similarly to the total fuel and emission costs presented in 6b, decreasing by around 0.33–0.94 % (0.90–2.54 MtCO₂).

As expected, the better accuracy of smaller time resolutions was seen to result in the lowest total yearly operational costs for most of the modelled forecast horizons. The differences in the total costs of the 12-hour and 24-hour time resolutions compared to the 6-hour resolution were relatively modest, between 0.00–0.05 % (–2–14 MEUR) and 0.04–0.10 % (11–28 MEUR) respectively. Even though the absolute values differ slightly between the used time resolutions, the overall trend in the different costs for the different forecast horizons remained quite similar. Interestingly, however, while the 6-hour time resolution resulted in the lowest total O&M and startup costs of all the tested resolutions, its fuel and emission costs were noticeably higher than those of the 12-hour and 24-hour resolutions.

The total electricity generation by source over the modelled year is presented in Figure 7a, with the changes compared to the 36 hours ahead forecast horizon highlighted in Figure 7b. The use of biomass could be seen to increase noticeably, by around 13–23 % (5–8 TWh), until a forecast horizon of 156 hours ahead. The increasing biomass generation replaced both coal and gas generation, decreasing them by around 5–8 % (3–6 TWh) and 1–4 % (2–6 TWh) respectively. Interestingly, while gas generation was observed to decrease until the longest modelled horizon of 348 hours ahead of time, coal generation reached its minimum at the 156 hour horizon, after which it was observed to slowly increase again.

Figure 8 presents the share of total curtailed wind power production, as well as total spilled hydropower relative to the yearly inflows, as a function of the modelled forecast horizon. Both the curtailment of wind power and hydropower spillage could be seen to decrease as the modelled forecast horizon increased. PV generation was not curtailed in any of the simulations due to it having the cheapest operational costs of all the modelled generation technologies. However, the wind and hydropower resources were already almost fully utilised before extending the forecast horizon, so the reductions in curtailment and spill remained modest around 0.10 pp. Unlike with the total yearly operational costs, no clear differences in wind power curtailment and

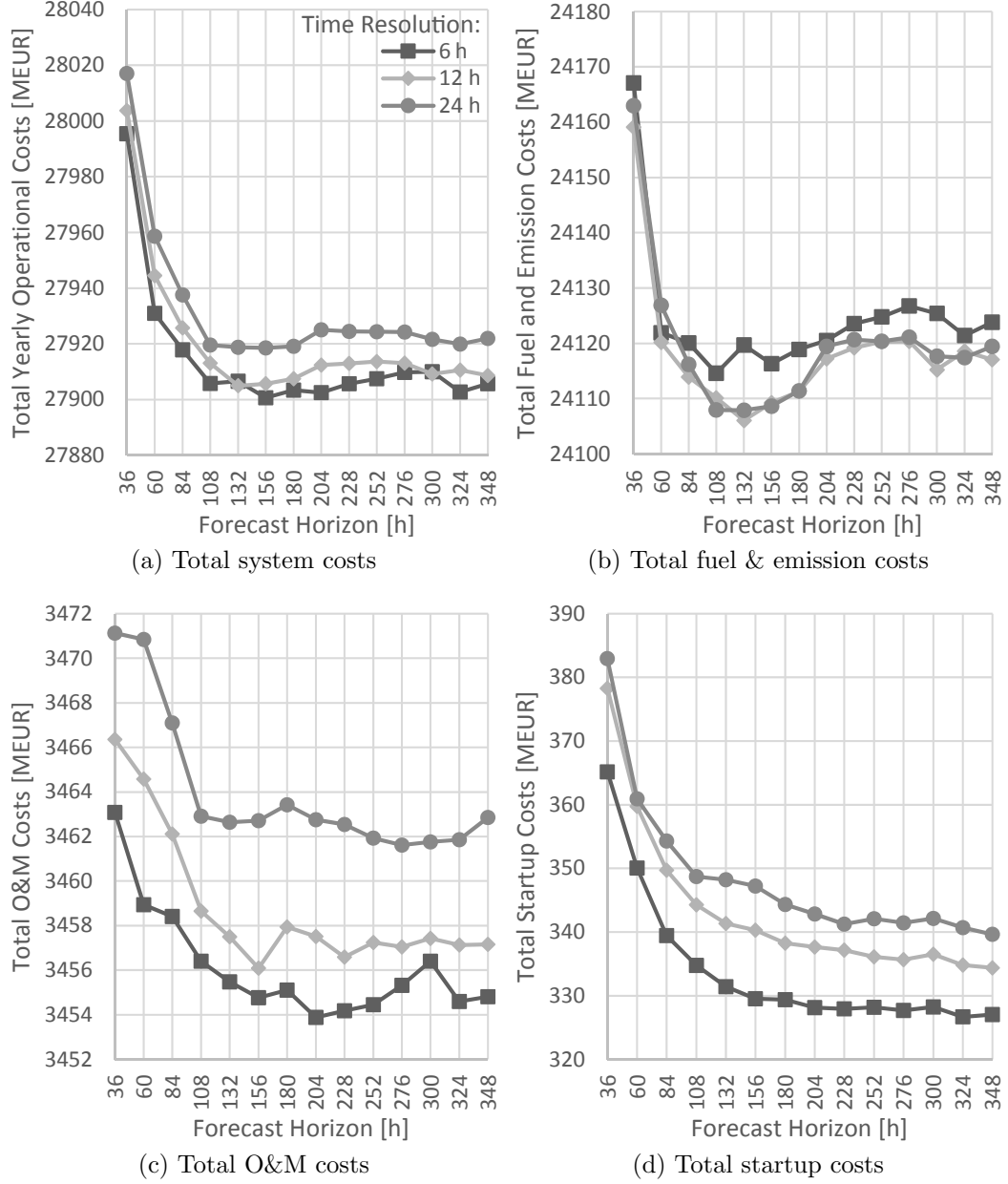
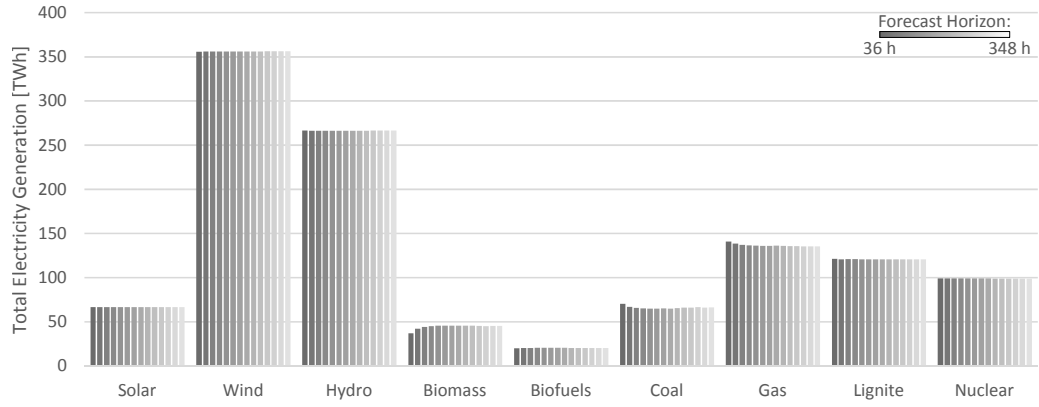
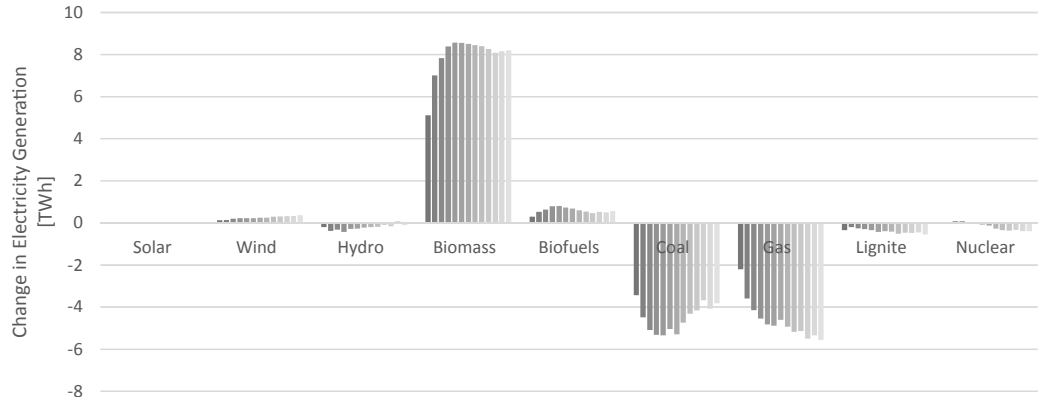


Figure 6: Total yearly operational costs (a) of the power system as a function of forecast horizon with multiple time resolutions, as well as a breakdown of the individual cost components. The fuel and emission costs (b) can be seen to account for the majority of the total costs, while the O&M (c) and startup (d) costs play less significant roles.



(a) Total yearly electricity generation by source



(b) Change compared to the 36 hour ahead forecast horizon

Figure 7: Total electricity generation by source for different modelled forecast horizons with 6-hour time resolution (a), and its changes compared to the 36 hours ahead forecast horizon (b). Darker shades of grey indicate a shorter forecast horizon. Oil-fired generation has been omitted due to negligible total generation levels below 1 GWh with all modelled forecast horizons.

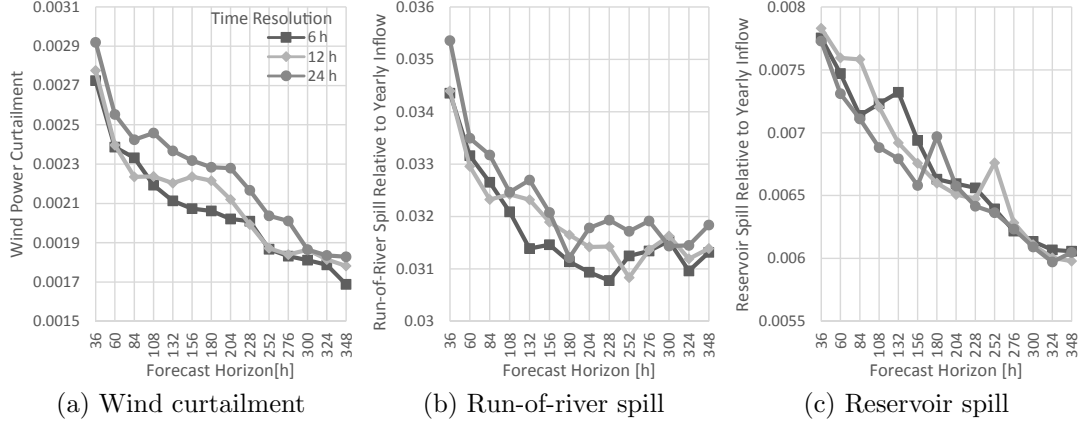


Figure 8: Share of total curtailed wind power production (a), as well as the total spilled run-of-river (b) and reservoir hydropower (c) relative to their yearly inflows as a function of forecast horizon with multiple time resolutions.

411 hydropower spillage between the different time resolutions could be seen.

412 Figure 9 presents the total energy in all the hydropower reservoirs over the
 413 simulations with different forecast horizons. The extended weather forecasts
 414 only have a barely noticeable impact on the total use of hydropower reser-
 415 voirs, although the relative differences in reservoir energy content between
 416 the horizons could be up to around 13–16 % in spring, when the reservoir lev-
 417 els were at their lowest. For individual reservoirs and especially for pumped
 418 hydro storage plants, the differences between the simulations were higher,
 419 but didn't seem to impact the overall use of reservoir energy.

420 4. Discussion

421 While the total yearly operational costs of the modelled power system
 422 could be seen to decrease when increasing the forecast horizon beyond 36
 423 hours typical of day-ahead simulations, the benefits rather quickly stagnated
 424 around forecast horizons of 132–156 hours. Most of the observed cost de-
 425 creases at forecast horizons between 36–132 hours due to the rapid decline
 426 in fuel and emission costs shown in Figure 6b, driven by cheaper biomass
 427 based generation replacing coal and gas based generation as seen from Fig-
 428 ure 7b. With longer forecast horizons of 132–348 hours, however, the total
 429 fuel and emission costs could be seen to slowly increase, along with coal based
 430 generation.

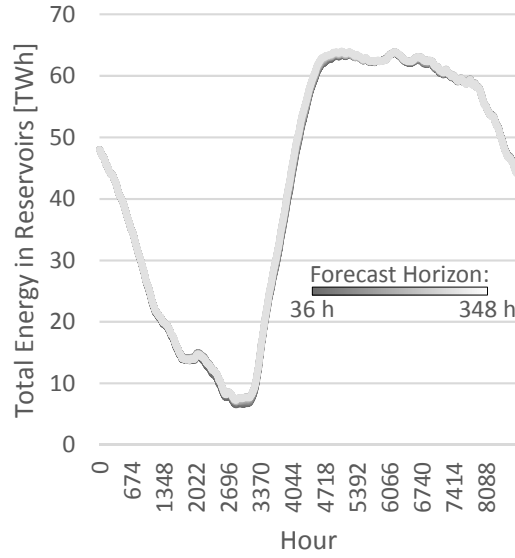


Figure 9: Total energy in all the hydropower reservoirs over the simulations with different forecast horizons using the 6-hour time resolution. Darker shades of grey indicate a shorter forecast horizon.

431 The observed increase in fuel and emission costs could potentially be ex-
 432 plained by the increasing spread of the quantile forecasts at longer horizons,
 433 as seen in the example forecasts presented in Figure 4. With sufficiently
 434 large forecast uncertainty at the end of the forecast horizon, the expected
 435 operational cost minimisation could favour excessively robust solutions, but
 436 determining the exact mechanism through which the costs were increased is
 437 challenging. While the model was observed keeping increasing amounts of
 438 idle capacity online on longer forecast horizons, slightly decreasing the aver-
 439 age efficiency of the generation fleet, this effect alone couldn't fully explain
 440 the observed increase in fuel and emission costs.

441 Another possible way for the model to brace itself for the perceived un-
 442 certainty could have been to use reservoir hydropower more sparingly. This
 443 was considered unlikely, however, as there were no significant differences ob-
 444 served in total stored reservoir energy as the forecast horizon was increased,
 445 as shown in Figure 9, nor in the total hydropower generation shown in Fig-
 446 ure 7b. Based on these results, it would indeed seem that accounting for
 447 short-term VRE variability in long-term hydro-thermal expansion planning
 448 [17, 19, 18] wouldn't result in significant differences on the long-term schedul-
 449 ing. However, in order to ascertain this, the long-term stochasticity in yearly

450 hydropower inflows would have to be properly accounted for in addition to
451 the short-term VRE variability. Furthermore, increasing the forecast horizon
452 length was observed to affect the operational strategies of differently sized
453 reservoirs individually. Even though the differences evened out when com-
454 paring the total reservoir energy of the system in the simulations, assessing
455 the implications of extended forecast horizons on energy storages of different
456 sizes could be a topic for further research.

457 All in all, the results show that there was some additional value in ex-
458 tending the forecast horizon beyond the day-ahead horizon of 24–36 hours
459 typically used in existing literature on stochastic UC&ED [11, 12, 13, 14, 21,
460 15, 20]. However, no clear savings were observed beyond forecast horizons of
461 around 132–156 hours ahead of time. It is also worth noting that since most
462 of the observed system cost savings were achieved via biomass replacing coal
463 and gas, the results are potentially quite sensitive to the fuel and carbon
464 price assumptions. Furthermore, while the observed decrease in CO₂ emis-
465 sions was not quite as negligible as the one in the study by Erichsen et al.
466 [22], it still remained relatively small compared to the total yearly emissions
467 of the modelled Nordic power system.

468 Increasing the modelled forecast horizon was observed to reduce both the
469 curtailment of wind power, as well as the spillage of reservoir and run-of-river
470 hydropower, as seen in Figure 8. However, the modelled power system was
471 large and flexible enough to be able to utilise most of these resources already
472 at the shortest modelled forecast horizon of 36 hours, making the reductions
473 in wind power curtailment and hydropower spillage largely negligible. The
474 impact of extended weather forecasts in decreasing wind power curtailment
475 and hydropower spillage could be more meaningful in a different case study
476 with a significant reliance on VRE generation, or in an isolated system. Such
477 case studies could be an interesting line of possible future work, along with
478 determining if improving the accuracy of the ensemble forecasts past the
479 132 hour mark would result in meaningful improvements for the optimal
480 scheduling of the power system.

481 Somewhat surprisingly, the overall trends in both the total yearly opera-
482 tional costs as well as the wind power curtailment and hydropower spillage
483 were found to be rather consistent across the 6-hour, 12-hour, and 24-hour
484 time resolutions. While each time resolution had noticeably different cost lev-
485 els, the costs behaved in a similar manner for all of the time resolutions when
486 the forecast horizon was increased. Since the simulations with the coarser
487 time resolutions didn’t affect the trends in the results, it would seem that

adjusting the time resolution could be useful e.g. for acquiring preliminary results in less time.

5. Conclusions

This work aimed to study the potential benefits of using extended weather forecasts for improving the hydro-thermal scheduling of hydro-dominated power systems. While the total yearly operational costs were seen to decrease as the modelled forecast horizon was increased beyond the typical day-ahead horizon of 36 hours until around 132–156 hours, the relative costs savings remained relatively small at around 0.20–0.35 % per year. Further cost reductions were not observed with forecast horizons between 156–348 hours, but further research is required to ascertain whether this is due to the increasing spread of the underlying ensemble weather forecasts, or due to the properties of the modelled power system.

Similarly, only slight decreases of around 0.10 pp in wind power curtailment and hydropower spillage were observed. However, the modelled Nordic power system was already able to utilise its wind and hydropower resources almost fully at the 36 hours ahead forecast horizon. Further research is required to see if extended weather forecasts could reduce wind power and hydropower spill in more isolated power systems, or in power systems with significantly higher dependance on VRE resources.

Acknowledgements

This study was supported by the Academy of Finland project “Improving the value of variable and uncertain power generation in energy systems (VaGe)” (grant number 284973), which is part of the New Energy programme; as well as by the Strategic Research Council at the Academy of Finland, project “Transition to a resource efficient and climate neutral electricity system (EL-TRAN)” (grant number 314319).

The hydropower inflow time series for Norway and Sweden were kindly provided by Linn Emelie Schäffer at SINTEF Energy AS.

Appendix A. Demand models

Generally, both electricity and heat demand on large enough scales are dependent on ambient temperatures due to e.g. direct electrical heating.

520 Additionally, both demands are also dependent on daily cycles due to societal
521 patterns, such as business days and industrial processes. In this work, the
522 electricity demand D_t^{elec} at time t was modelled using a generalised additive
523 model

$$\mathbb{E}[D_t^{\text{elec}}] = f_1(T_t) + f_2(H_t) + f_3(B_t) + f_4(m_t) + \beta_0, \quad (\text{A.1})$$

524 where T_t is the ambient temperature, H_t is the hour of the day, B_t is a boolean
525 for business days, m_t is the month, and β_0 is a constant. The penalized B-
526 spline functions from $f_{1,\dots,4}$ were estimated using pyGAM [44]. Similarly, the
527 heat demand D_t^{heat} followed

$$\mathbb{E}[D_t^{\text{heat}}] = f_1(T_{t,\text{MA24}}) + f_2(T_t) + f_3(H_t) + f_4(W_t) + f_5(m_t) + \beta_0, \quad (\text{A.2})$$

528 where $T_{t,\text{MA24}}$ is the 24-hour moving average of the ambient temperature T_t ,
529 and W_t is the weekday. Tables A.3 and A.4 present the bias, MAE, and
530 standard deviation of the errors in the electricity and heat demand models
531 respectively.

Table A.3: Bias, MAE and standard deviation (sd) of errors of the electricity demand model in Equation (A.1). The values are given as per units from the peak demand.

country	bias/ 10^{-12}	MAE	sd
DE	1.005	0.041	0.055
DK	0.660	0.025	0.032
EE	0.934	0.030	0.039
FI	1.028	0.020	0.026
LT	1.018	0.033	0.043
LV	0.970	0.035	0.045
NO	0.857	0.017	0.024
PL	1.051	0.036	0.052
SE	0.912	0.023	0.030

532 Appendix B. Power curve model

533 The per unit wind power conversion from wind speed to power can be
534 expressed as

$$P_{\text{pu}}(w) = \frac{1}{2S_r} \rho w^3 c_p, \quad (\text{B.1})$$

Table A.4: Bias, MAE and standard deviation (sd) of errors of the heat demand model in Equation (A.2). The values are given as per units from the peak demand.

heat area	bias/ 10^{-12}	MAE	sd
DK_W_Rural	0.256	0.042	0.056
SE_M_Urban	0.219	0.060	0.076
SE_M_Rural	0.099	0.061	0.076
FI_R_Rural	0.302	0.050	0.066
SE_N_Rural	0.206	0.062	0.078
DE_All	0.206	0.025	0.033
DK_E_Urban	0.205	0.039	0.054
SE_S_Rural	0.188	0.061	0.077
FI_R_Urban	0.276	0.057	0.071

where Sr is specific rating, which is the rated power divided by the swept area of the rotor $Sr = P_{\max} / A$, ρ is the density of the air, w is the wind speed at the desired height and c_p is the coefficient of the performance. An important parameter that can be derived from Equation (B.1) is the rated wind speed

$$w_{\text{rated}} = \sqrt[3]{\frac{2Sr}{\rho c_p}}, \quad (\text{B.2})$$

showing that by lowering the specific rating or by increasing c_p , the rated wind speed can be lowered. As the wind speed increases, the wind speed reaches a cut-off wind speed, $w_{\text{cut-off}}$ which after the power production is run down. The power curve model in this work assumed that the power production was run down linearly from $P_{\text{pu}}(w_{\text{cut-off}} - w_{\text{cut-off},\Delta}) = 1$ to $P_{\text{pu}}w_{\text{cut-off}} + w_{\text{cut-off},\Delta} = 0$. Furthermore, $w_{\text{cut-off}}$ was assumed to be equal to 22 m/s and the hysteresis parameter $w_{\text{cut-off},\Delta}$ was assumed to be equal to 1 m/s.

However, Equation (B.1) has two major drawbacks: first, the equation assumes that the wind resource has no turbulence, and second, the ERA5 wind speed data has 0.25° spatial resolution and the value must correspond to the total wind power production over the wind power plants in the 0.25° grid. Following the methodology in [40], a Gaussian filter was used to smooth the power curve in (B.1) according to

$$P(w, \delta_w, \sigma) = \int_{v=0}^{\infty} P_{\text{pu}}(v + \delta_w) f(v, w, \sigma) dv, \quad (\text{B.3})$$

553 where $f(v, w, \sigma)$ is the probability density function of a normal distribution
 554 with mean w and standard deviation σ , and δ_w is a correction constant
 555 for the wind speed. It was assumed that the standard deviation follows the
 556 equation $\sigma = Iw$, where I is the turbulence intensity. In practice, the integral
 557 in Equation (B.3) was discretised and the upper limit for the sum was 50 m/s.

558 The zero turbulence power curve $P_{pu}(w)$ and it's c_p can be calculated
 559 using a method presented in [46], which is based on iterating Equation (B.3)
 560 and assumes that the zero turbulence power curve has a constant c_p between
 561 cut-in and rated wind speed. In theory, the state-of-the-art variable speed
 562 wind power plants can operate with optimal c_p by operating the turbine at
 563 the optimal tip-speed ratio by regulating the pitch angle. In this work, zero
 564 turbulence curves were solved for five different wind power technologies used
 565 in ten different wind power plants in Finland using sales power curves, which
 566 are standardised using IEC standard [46] $\rho = 1.225 \text{ kg/m}^3$ and turbulence
 567 intensity $I = 0.1w$. These zero turbulence power curves were assumed to be
 568 reasonable for the other modelled countries as well, and were used for all of
 569 the modelled power system regions.

570 Additionally, since the turbulence intensity in the ERA5 data is unknown,
 571 the standard deviation in the Gaussian filter was estimated as

$$\sigma(a, b) = a + bw_{\text{ERA}}, \quad (\text{B.4})$$

572 following the methodology in [47]. The values for the parameters a , b and δ_w
 573 were determined by minimising the weighted absolute error over time t , using
 574 weights $u(w_t)$ from the wind speed distribution probability density function
 575 and using ERA5 wind speeds from 100 meters

$$\min_{\delta_w, a, b} \sum_{t=1}^{8760} u(w_{\text{ERA}, t}) |\Phi_t - P(w_{\text{ERA}, t}, \delta_w, a, b)|, \quad (\text{B.5})$$

576 resulting in $a = 0.35$ and $b = 0.075$, where Φ_t was the measured wind power
 577 production from the Finnish wind power plant. The wind speed correction
 578 term δ_w varied from site to site, and it's main purpose was to correct bias
 579 between the ERA5 and actual wind speeds, such that the parameters a and
 580 b from different sites and wind power technologies were comparable. This all
 581 results into the power curve model

$$P(w) = P_{pc}(Sr, c_p, \rho, w, w_{\text{cut-off}}, w_{\text{cut-off}, \Delta}). \quad (\text{B.6})$$

References

- [1] M. Lei, L. Shiyan, J. Chuanwen, L. Hongling, Z. Yan, A review on the forecasting of wind speed and generated power, *Renewable and Sustainable Energy Reviews* 13 (4) (2009) 915–920. doi:10.1016/j.rser.2008.02.002.
- [2] J. Antonanzas, N. Osorio, R. Escobar, R. Urraca, F. J. Martinez-de pison, F. Antonanzas-torres, Review of photovoltaic power forecasting, *Solar Energy* 136 (2016) 78–111. doi:10.1016/j.solener.2016.06.069. Available at: <http://dx.doi.org/10.1016/j.solener.2016.06.069>
- [3] E. B. Ssekulima, M. B. Anwar, A. Al Hinai, M. S. El Moursi, Wind speed and solar irradiance forecasting techniques for enhanced renewable energy integration with the grid: a review, *IET Renewable Power Generation* 10 (7) (2016) 885–989. doi:10.1049/iet-rpg.2015.0477.
- [4] G. Notton, M. L. Nivet, C. Voyant, C. Paoli, C. Darras, F. Motte, A. Fouilloy, Intermittent and stochastic character of renewable energy sources: Consequences, cost of intermittence and benefit of forecasting, *Renewable and Sustainable Energy Reviews* 87 (December 2016) (2018) 96–105. doi:10.1016/j.rser.2018.02.007. Available at: <https://doi.org/10.1016/j.rser.2018.02.007>
- [5] A. Ahmed, M. Khalid, A review on the selected applications of forecasting models in renewable power systems, *Renewable and Sustainable Energy Reviews* 100 (September 2018) (2019) 9–21. doi:10.1016/j.rser.2018.09.046. Available at: <https://doi.org/10.1016/j.rser.2018.09.046>
- [6] A. Agüera-Pérez, J. C. Palomares-Salas, J. J. González de la Rosa, O. Florencias-Oliveros, Weather forecasts for microgrid energy management: Review, discussion and recommendations, *Applied Energy* 228 (June) (2018) 265–278. doi:10.1016/j.apenergy.2018.06.087. Available at: <https://doi.org/10.1016/j.apenergy.2018.06.087>
- [7] Y. Ren, P. N. Suganthan, N. Srikanth, Ensemble methods for wind and solar power forecasting - A state-of-the-art review, *Renewable and Sustainable Energy Reviews* 50 (2015) 82–91. doi:10.1016/j.rser.2015.04.081. Available at: <http://dx.doi.org/10.1016/j.rser.2015.04.081>

- [8] Q. P. Zheng, J. Wang, A. L. Liu, Stochastic Optimization for Unit Commitment - A Review, *IEEE Transactions on Power Systems* 30 (4) (2015) 1913–1924. doi:10.1109/TPWRS.2014.2355204.
- [9] W. van Ackooij, I. Danti Lopez, A. Frangioni, F. Lacalandra, M. Tahanan, Large-scale unit commitment under uncertainty: an updated literature survey, *Annals of Operations Research* 271 (1) (2018) 11–85. doi:10.1007/s10479-018-3003-z.
Available at: <https://doi.org/10.1007/s10479-018-3003-z>
- [10] M. Håberg, Fundamentals and recent developments in stochastic unit commitment, *International Journal of Electrical Power and Energy Systems* 109 (February) (2019) 38–48. doi:10.1016/j.ijepes.2019.01.037.
Available at: <https://doi.org/10.1016/j.ijepes.2019.01.037>
- [11] J. Wang, A. Botterud, R. Bessa, H. Keko, L. Carvalho, D. Issicaba, J. Sumaili, V. Miranda, Wind power forecasting uncertainty and unit commitment, *Applied Energy* 88 (11) (2011) 4014–4023. doi:10.1016/j.apenergy.2011.04.011.
Available at: <http://dx.doi.org/10.1016/j.apenergy.2011.04.011>
- [12] E. V. Mc Garrigle, P. G. Leahy, Quantifying the value of improved wind energy forecasts in a pool-based electricity market, *Renewable Energy* 80 (2015) 517–524. doi:10.1016/j.renene.2015.02.023.
Available at: <http://dx.doi.org/10.1016/j.renene.2015.02.023>
- [13] Q. Wang, C. B. Martinez-Anido, H. Wu, A. R. Florita, B. M. Hodge, Quantifying the Economic and Grid Reliability Impacts of Improved Wind Power Forecasting, *IEEE Transactions on Sustainable Energy* 7 (4) (2016) 1525–1537. doi:10.1109/TSTE.2016.2560628.
- [14] E. A. Bakirtzis, P. N. Biskas, Multiple Time Resolution Stochastic Scheduling for Systems With High Renewable Penetration, *IEEE Transactions on Power Systems* 32 (2) (2017) 1030–1040. doi:10.1109/TPWRS.2016.2574645.
- [15] E. A. Bakirtzis, C. K. Simoglou, P. N. Biskas, A. G. Bakirtzis, Storage management by rolling stochastic unit commitment for high renewable energy penetration, *Electric Power Systems Research* 158 (2018) 240–249. doi:10.1016/j.epsr.2017.12.025.
Available at: <http://dx.doi.org/10.1016/j.epsr.2017.12.025>

- [16] A. R. De Queiroz, Stochastic hydro-thermal scheduling optimization: An overview, *Renewable and Sustainable Energy Reviews* 62 (2016) 382–395. doi:10.1016/j.rser.2016.04.065.
Available at: <http://dx.doi.org/10.1016/j.rser.2016.04.065>
- [17] A. Helseth, A. Gjelsvik, B. Mo, Ú. Linnet, A model for optimal scheduling of hydro thermal systems including pumped-storage and wind power, *IET Generation, Transmission & Distribution* 7 (12) (2013) 1426–1434. doi:10.1049/iet-gtd.2012.0639.
- [18] A. Helseth, B. Mo, A. Lote Henden, G. Warland, Detailed long-term hydro-thermal scheduling for expansion planning in the Nordic power system, *IET Generation, Transmission & Distribution* 12 (2) (2017) 441–447. doi:10.1049/iet-gtd.2017.0903.
- [19] S. R. Silva, A. R. De Queiroz, L. M. M. Lima, J. W. M. Lima, Effects of wind penetration in the scheduling of a hydro-dominant power system, *IEEE Power and Energy Society General Meeting 2014-Octob (October)*. doi:10.1109/PESGM.2014.6939121.
- [20] S. E. Razavi, A. Esmaeel Nezhad, H. Mavalizadeh, F. Raeisi, A. Ahmadi, Robust hydrothermal unit commitment: A mixed-integer linear framework, *Energy* 165 (2018) 593–602. doi:10.1016/j.energy.2018.09.199.
Available at: <https://doi.org/10.1016/j.energy.2018.09.199>
- [21] G. E. Alvarez, M. G. Marcovecchio, P. A. Aguirre, Security-Constrained Unit Commitment Problem including thermal and pumped storage units: An MILP formulation by the application of linear approximations techniques, *Electric Power Systems Research* 154 (2018) 67–74. doi:10.1016/j.epsr.2017.07.027.
Available at: <https://doi.org/10.1016/j.epsr.2017.07.027>
- [22] G. Erichsen, T. Zimmermann, A. Kather, Effect of Different Interval Lengths in a Rolling Horizon MILP Unit Commitment with Non-Linear Control Model for a Small Energy System, *Energies* 12 (6) (2019) 1003. doi:10.3390/en12061003.
Available at: <https://www.mdpi.com/1996-1073/12/6/1003>
- [23] J. J. Miettinen, J. Ikaheimo, T. Rasku, H. Holttinen, J. Kiviluoma, Impact of longer stochastic forecast horizon on the operational cost of

- 683 a power system, in: International Conference on the European Energy
684 Market, EEM, IEEE, Lodz, 2018. doi:10.1109/EEM.2018.8469219.
- 685 [24] N. Helistö, J. Kiviluoma, J. Ikäheimo, T. Rasku, E. Rinne, C. O'Dwyer,
686 R. Li, D. Flynn, Backbone – an adaptable energy systems modelling
687 framework, to be submitted (2019).
688 Available at: [https://cris.vtt.fi/en/publications/
689 backbone-an-adaptable-energy-systems-modelling-framework](https://cris.vtt.fi/en/publications/backbone-an-adaptable-energy-systems-modelling-framework)
- 690 [25] Directorate-General for Energy, Energy Modelling - EU Reference
691 Scenario 2016 (2016).
692 Available at: [https://data.europa.eu/euodp/data/dataset/
693 energy-modelling](https://data.europa.eu/euodp/data/dataset/energy-modelling)
- 694 [26] European Network of Transmission System Operators for Electricity
695 (ENTSO-E), TYNDP 2018 (2018).
696 Available at: <https://tyndp.entsoe.eu/tyndp2018/>
- 697 [27] e Highway 2050 consortium, e-Highway2050 Results (2013).
698 Available at: <http://www.e-highway2050.eu/results/>
- 699 [28] P. Meibom, R. Barth, I. Norheim, H. Ravn, P. Sørensen, Wind Power
700 Integration in a Liberalised Electricity Market - WILMAR Final
701 Technical Report, Tech. rep., Risoe National Laboratory, Roskilde
702 (2006).
703 Available at: [http://www.wilmar.risoe.dk/Deliverables/
704 WilmarFinalTechnicalReportPublic.pdf](http://www.wilmar.risoe.dk/Deliverables/WilmarFinalTechnicalReportPublic.pdf)
- 705 [29] D. R. Gómez, J. D. Watterson, B. B. Americanohia, C. Ha, G. Mar-
706 land, E. Matsika, L. N. Namayanga, B. Osman-Elasha, J. D. K. Saka,
707 K. Treanton, Stationary Combustion, in: S. Eggleston, L. Buendia,
708 K. Miwa, T. Ngara, K. Tanabe (Eds.), 2006 IPCC Guidelines for
709 National Greenhouse Gas Inventories, Institute for Global Environ-
710 mental Strategies (IGES), Hayama, Kanagawa, 2006, Ch. 2, p. 47.
711 arXiv:arXiv:1011.1669v3, doi:10.1016/S0166-526X(06)47021-5.
712 Available at: [http://www.ipcc-nggip.iges.or.jp/public/2006gl/pdf/2_
713 Volume2/V2_2_Ch2_Stationary_Combustion.pdf](http://www.ipcc-nggip.iges.or.jp/public/2006gl/pdf/2_Volume2/V2_2_Ch2_Stationary_Combustion.pdf)
- 714 [30] Pöyry Management Consulting Oy, Suomen sähkötehon riittävyys ja
715 kapasiteettirakenteen kehitys vuoteen 2030 (Capacity adequacy and the

- 716 future development of generation capacity until 2030 in Finland), Tech.
717 rep., Pöyry Management Consulting Oy, Vantaa (2015).
- 718 [31] European Commission, Excise Duty on Energy (2003).
719 Available at: [https://ec.europa.eu/taxation_customs/business/](https://ec.europa.eu/taxation_customs/business/excise-duties-alcohol-tobacco-energy/excise-duties-energy_en)
720 [excise-duties-alcohol-tobacco-energy/excise-duties-energy_en](https://ec.europa.eu/taxation_customs/business/excise-duties-alcohol-tobacco-energy/excise-duties-energy_en)
- 721 [32] P. Andreasen, T. Toivonen, O. H. Hoelsaeter, J. Magnusson, AGREE-
722 MENT (Translation) regarding operation of the interconnected Nordic
723 power system (System Operation Agreement), Tech. Rep. 13, European
724 Network of Transmission System Operators for Electricity (ENTSO-E),
725 Stockholm (2006).
- 726 [33] UCTE Secretariat, OH Team, Continental Europe Operation Handbook
727 (2004).
728 Available at: [https://www.entsoe.eu/publications/](https://www.entsoe.eu/publications/system-operations-reports/#continental-europe-operation-handbook)
729 [system-operations-reports/#continental-europe-operation-handbook](https://www.entsoe.eu/publications/system-operations-reports/#continental-europe-operation-handbook)
- 730 [34] ENTSO-E, ENTSO-E Transparency Platform (2018).
731 Available at: <https://transparency.entsoe.eu>
- 732 [35] O. Wolfgang, A. Haugstad, B. Mo, A. Gjelsvik, I. Wangensteen,
733 G. Doorman, Hydro reservoir handling in Norway before and after
734 deregulation, Energy 34 (10) (2009) 1642–1651.
735 Available at: [http://www.sciencedirect.com/science/article/](http://www.sciencedirect.com/science/article/B6V2S-4X1R2RK-2/2/fecd77eed29794b5b17299691ec3fbdc)
736 [B6V2S-4X1R2RK-2/2/fecd77eed29794b5b17299691ec3fbdc](http://www.sciencedirect.com/science/article/B6V2S-4X1R2RK-2/2/fecd77eed29794b5b17299691ec3fbdc)
- 737 [36] Finnish Environmental Administration, Hydrology and water resources
738 information system HYDRO (2018).
739 Available at: <https://wwwp2.ymparisto.fi/scripts/hearts/welcome.asp>
- 740 [37] Copernicus Climate Change Service (C3S), ERA5: Fifth generation of
741 ECMWF atmospheric reanalyses of the global climate. Copernicus Cli-
742 mate Change Service Climate Data Store (CDS) (2019).
743 Available at: <https://cds.climate.copernicus.eu/cdsapp>
- 744 [38] European Centre for Medium-Range Weather Forecasts (ECMWF), Set
745 III - Atmospheric model Ensemble 15-day forecast (ENS) (2018).
746 Available at: <https://www.ecmwf.int/en/forecasts/datasets/set-iii>

- 747 [39] Portland State Aerospace Society, A Quick Derivation relating altitude
748 to air pressure, Tech. rep., Portland State Aerospace Society (Dec. 2004).
749 Available at: [https://web.archive.org/web/20110928003908/http://](https://web.archive.org/web/20110928003908/http://psas.pdx.edu/RocketScience/PressureAltitude.Derived.pdf)
750 [psas.pdx.edu/RocketScience/PressureAltitude.Derived.pdf](https://web.archive.org/web/20110928003908/http://psas.pdx.edu/RocketScience/PressureAltitude.Derived.pdf)
- 751 [40] P. Nørgaard, H. Holttinen, A Multi-Turbine Power Curve Approach, in:
752 Proceedings of the Nordic Wind Power Conference NWPC'04, Gothen-
753 burg, 2004.
- 754 [41] S. Pfenninger, I. Staffell, Long-term patterns of European PV output
755 using 30 years of validated hourly reanalysis and satellite data, *Energy*
756 114 (2016) 1251–1265. doi:10.1016/j.energy.2016.08.060.
- 757 [42] The Wind Power, Wind Farms database, version 2017-12-07 (2017).
758 Available at: <https://www.thewindpower.net/index.php>
- 759 [43] Open Power System Data, Data Package: Renewable power plants
760 (2018).
761 Available at: <https://open-power-system-data.org/>
- 762 [44] D. Servén, C. Brummitt, H. Abedi, pyGAM: Generalized Additive Mod-
763 els in Python (2018). doi:10.5281/zenodo.1476122.
764 Available at: <https://zenodo.org/record/1476122#.XOfBnmNRVaQ>
- 765 [45] J. Kiviluoma, E. Rinne, T. Rasku, N. Helistö, Backbone - An adaptable
766 energy system model (2018).
767 Available at: <https://gitlab.vtt.fi/backbone/backbone>
- 768 [46] IEC, IEC 61400-12-1 Power performance measurements of electricity
769 producing wind turbines, Tech. rep., IEC (2017).
- 770 [47] I. Staffell, S. Pfenninger, Using bias-corrected reanalysis to simulate
771 current and future wind power output, *Energy* 114 (2016) 1224–1239.
772 doi:10.1016/j.energy.2016.08.068.
773 Available at: [http://linkinghub.elsevier.com/retrieve/pii/](http://linkinghub.elsevier.com/retrieve/pii/S0360544216311811)
774 [S0360544216311811](http://linkinghub.elsevier.com/retrieve/pii/S0360544216311811)